Science in China Series D: Earth Sciences

www.scichina.com
earth.scichina.com
www.springerlink.com

GPS-constrained inversion of present-day slip rates along major faults of the Sichuan-Yunnan region, China

WANG YanZhao[1], WANG EnNing[2], SHEN ZhengKang[1†], WANG Min[3], GAN WeiJun[1], QIAO XueJun[4], MENG GuoJie[3], LI TieMing[1], TAO Wei[1], YANG YongLin[5], CHENG Jia[1] & LI Peng[3]

[1] State Key Laboratory of Earthquake Dynamics, Institute of Geology, China Earthquake Administration, Beijing 100029, China;
[2] School of Earth and Space Sciences, University of Science and Technology of China, Hefei 230026, China;
[3] Institute of Earthquake Science, China Earthquake Administration, Beijing 100036, China;
[4] Institute of Seismology, China Earthquake Administration, Wuhan 430071, China;
[5] Survey Engineering Institute of Earthquake Administration of Sichuan Province, Ya'an 625000, China

A linked-fault-element model is employed to invert for contemporary slip rates along major active faults in the Sichuan-Yunnan region (96°—108°E, 21°—35°N) using the least squares method. The model is based on known fault geometry, and constrained by a GPS-derived horizontal velocity field. Our results support a model attributing the eastward extrusion of the Tibetan Plateau driven mainly by the north-northeastward indentation of the Indian plate into Tibet and the gravitational collapse of the plateau. Resisted by a relatively stable south China block, materials of the Sichuan-Yunnan region rotate clockwise around the eastern Himalayan tectonic syntaxis. During the process the Garzê-Yushu, Xianshuihe, Anninghe, Zemuhe, Daliangshan, and Xiaojiang faults, the southwest extension of the Xiaojiang fault, and the Daluo-Jinghong and Mae Chan faults constitute the northeast and east boundaries of the eastward extrusion, with their left slip rates being 0.3—14.7, 8.9—17.1, 5.1±2.5, 2.8±2.3, 7.1±2.1, 9.4±1.2, 10.1±2.0, 7.3±2.6, and 4.9±3.0 mm/a respectively. The southwestern boundary consists of a widely distributed dextral transpressional zone other than a single fault. Right slip rates of 4.2±1.3, 4.3±1.1, and 8.5±1.7 mm/a are detected across the Nanhua-Chuxiong-Jianshui, Wuliangshan, and Longling-Lancang faults. Crustal deformation across the Longmenshan fault is weak, with shortening rates of 1.4±1.0 and 1.6±1.3 mm/a across the Baoxing-Beichuan and Beichuan-Qingchuan segments. Northwest of the Longmenshan fault lies an active deformation zone (the Longriba fault) with 5.1±1.2 mm/a right slip across. Relatively large slip rates are detected across a few faults within the Sichuan-Yunnan block: 4.4±1.3 mm/a left slip and 2.7±1.1 mm/a shortening across the Litang fault, and 2.7±2.3 mm/a right-lateral shearing and 6.7±2.3 mm/a shortening across the Yunongxi fault and its surrounding regions. In conclusion, we find that the Sichuan-Yunnan region is divided into more than a dozen active micro-blocks by a large number of faults with relatively slow slip rates. The eastward extrusion of the Tibetan Plateau is absorbed and adjusted in the region mainly by these faults, other than a small number of large strike-slip faults with fast slip rates.

Sichuan-Yunnan region, GPS, linked-fault-element, slip rate

1 Introduction

The Sichuan-Yunnan region is located at the eastern margin of the Tibetan Plateau. Because of the north-northeastward indentation of the Indian plate into the Chinese continent, the region has become a frontal deformation zone to absorb the eastward extrusion of the

Received September 1, 2007; accepted June 10, 2008
doi: 10.1007/s11430-008-0106-4
†Corresponding author (email: zshen@ies.ac.cn)
Supported by the National Basic Research Program of China (Grant No. 2004CB418403), the Key Program of the National Natural Science Foundation of China (Grant No. 40334042), and the China Earthquake Administration Research Fund (Grant No. 200708002)

plateau, and has developed a rather unique tectonic setting and a complex fault system. The region has been hit frequently by strong earthquakes, and threatened seriously by seismic hazard potential. All of the unique aspects mentioned above have made the Sichuan-Yunnan region an ideal place for conducting research and testing models and hypotheses on the origin and evolution of the Tibetan Plateau, its associated crustal deformation mechanisms, and seismogenic processes and earthquake migration mechanisms, etc.

In the Sichuan-Yunnan region along boundaries of tectonic blocks, there exist three sets of active faults trending NW, NE, and nearly N-S, which also dictate the locations of catastrophic earthquakes[1] (Figure 1). These faults constitute four arch-shaped fault zones: the Xianshuihe-Xiaojiang, Jinsha River-Red River, Lan-

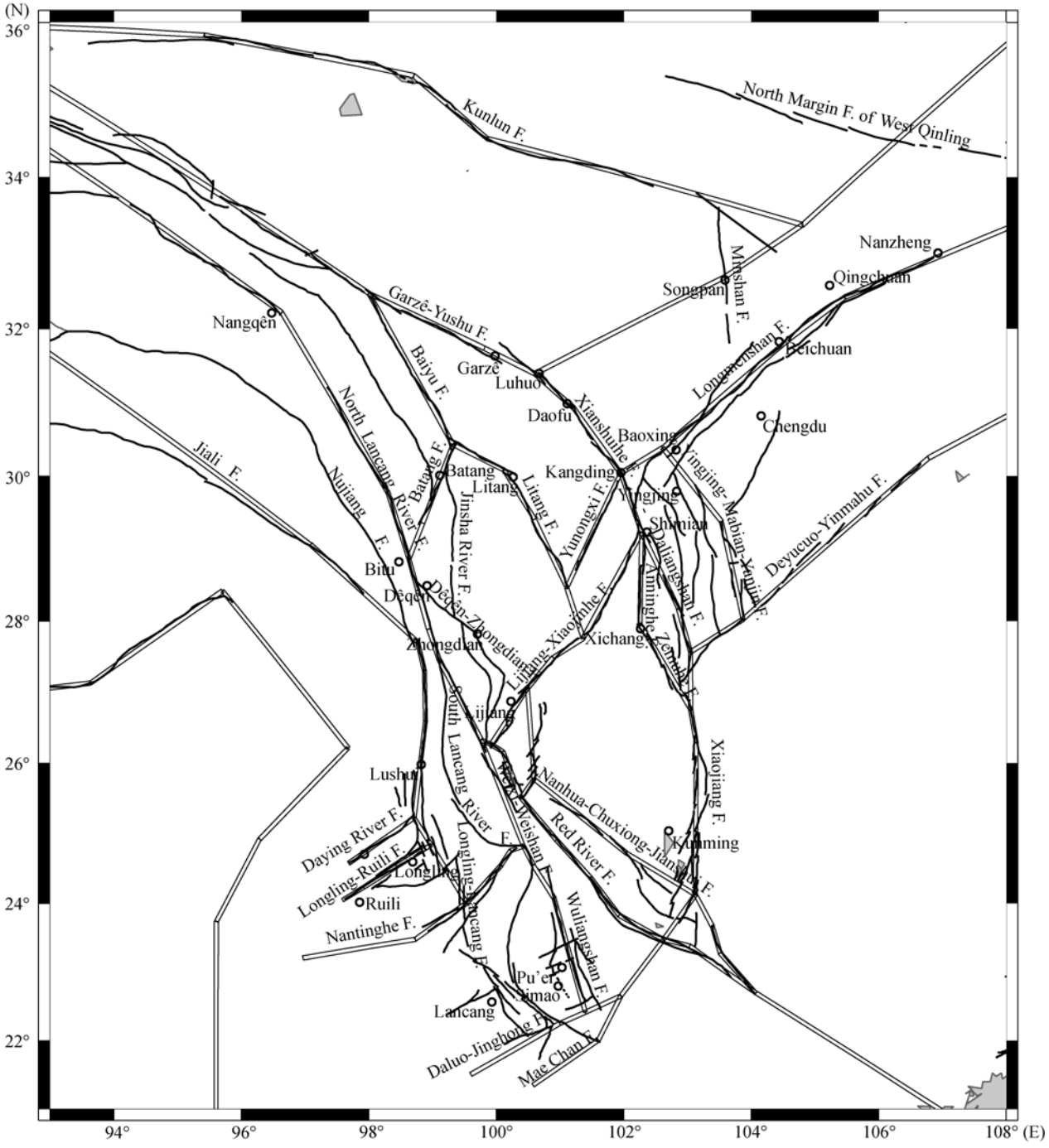

Figure 1 Tectonic map and fault model of the Sichuan-Yunnan region. F., fault.

cang-Weixi-Weishan-Wuliangshan, and Nujiang-Longling-Lancang fault zones. The NE trending faults include the Longmenshan and Lijiang-Xiaojinhe faults. Plenty of work has been done in the past about regional geology and deformation[2−18], resulting in abundant information for our model setup and testing of the modeling results.

Debate has been going on for decades about the mechanisms of uplifting and tectonic evolution of the Tibetan Plateau. Two end-member hypotheses exist. The "continental escape" hypothesis claims that the continental lithosphere is composed of a collage of large-scale rigid blocks and crustal deformation takes place mainly along block boundaries delineated by large-scale strike-slip faults which cut through the whole lithosphere. The eastward extrusion of the Tibetan Plateau is believed to be realized by the rapid slip along these faults[19−25]. The "continuous deformation" hypothesis believes that tectonic deformation of continental plates is characterized by widely distributed deformation. Therefore, collision between the Indian plate and Tibet is absorbed by the shortening and thickening of the Tibetan and Tianshan Mountains crust[26−30]. Thatcher[31] pointed out that the two alternative end-member models converge as the block size decreases. In fact, rheological structure of the continental lithosphere changes along with the variation of continental thickness, resulting in variation of crustal deformation pattern. In general, strength of the lower crust is relatively higher in the region with thinner lithosphere, making deformation between the upper and lower crusts more "coupled". Therefore the lithosphere behaves more as a quasi-rigid body, which may be well explained by the "continental escape" hypothesis. On the other hand, the lower crust is relatively weaker in areas with thicker lithosphere, making deformation between the upper and lower crusts more "decoupled". Driven by the flow of a weak lower crust, the brittle upper crust behaves more like "continuous deformation", which may well be explained by the "continuous deformation" hypothesis. When the thickness of the lithosphere is in between the two end-member cases, crustal deformation pattern becomes complex, not easily explained by either of the two alternative end-member models[31]. All the models, regardless of their bases, have predictions about fault slip rates, which can be compared directly with observations when available. We have acquired a GPS velocity field in the Sichuan-Yunnan region, and attempted to invert the data for slip rates of main active faults, thus providing constraints on differentiating those deformation models.

In recent years GPS techniques have gained rapid developments and have been applied repeatedly in studies on crustal deformation in the Sichuan-Yunnan region[8,32−37]. Shen et al.[8] used GPS data and inverted for the slip rates of main faults in the Sichuan-Yunnan region employing a multi-fault dislocation model. Shen et al.[36] calculated the slip rates of major faults from GPS velocity profiles based on a rigid block motion model. These models emphasized the role of either the fault slip or block motion on crustal deformation. The linked-fault-element model introduced in this study, on the other hand, balances a tradeoff between the block motion and fault slip, and at the same time takes into account of the continuous deformation in the vicinity of each fault induced by its locking effect, providing a better approximation of the real crustal deformation. In this study we use the most recent GPS observation results to infer slip rates of major faults in the Sichuan-Yunnan region, especially those faults in focused areas and/or areas with potential seismic risk not constrained by data so far. We also analyze the deformation pattern and its possible mechanisms. Our results can provide observational criterions for differentiating models about continental deformation and uplifting mechanisms of the Tibetan Plateau; at the same time, they can also serve the studies on seismic activities and provide an essential dataset for assessing earthquake potentials.

2 GPS data and processing

GPS data used in this study are mainly from the Crustal Motion Observation Network of China (CMONOC) project observed in 1999, 2001, and 2004 in the Sichuan-Yunnan region. They also include data from the A-level and B-level networks deployed by the Bureau of Surveying and Mapping under the Headquarters of the General Staff of PLA[38], data observed by survey teams from the China Earthquake Administration in 2002—2003 during the postseismic survey of the 2001 *Ms* 8.1 Kunlun Mountain Pass West earthquake[39], data collected by survey teams from the China Earthquake Administration in 2002—2003 during the emergency response survey along the "north-south seismic belt", and

data observed in 2005－2006 in reoccupation of some survey mode sites under the national basic key research project, "Physical Process and Strong Earthquake Prediction along Boundaries of Active Blocks", supported by Ministry of Science and Technology of China.

The GPS data were analyzed in three steps[38,40]. First, the GPS carrier phase data from the survey mode and continuous sites of CMONOC were processed together to obtain loosely constrained daily solutions for station positions and satellite orbits using the GAMIT software. Second, the regional daily solutions were combined with global solutions produced by the Scripps Orbital and Permanent Array Center (SOPAC) using the GLOBK software. Third, the station positions and velocities were estimated using the QOCA software. In the last step, we also took into account of the coseismic displacement effects of the 2001 Kunlun Mountain Pass West earthquake and the 2004 Sumatra earthquake by allowing station coseismic jumps at the epochs of the events[41]. The precision of the results was determined in two steps. First, single daily solutions and combined solutions were obtained with adequate assumption on GPS carrier phase errors. Second, the combined daily solutions were reweighted using the solution postfit residual RMS, so that the weighted postfit residual χ^2 equals the difference between the number of degrees of freedom in the data space and that in the parameter space, thus the solution uncertainties are equivalent to the standard deviations obtained from statistics. The GPS velocity field in the Sichuan-Yunnan region thus derived and used in this study is shown in Figure 2.

3 Linked-fault-element model

The most commonly used crustal deformation models so far are the rigid block motion model and the fault dislocation model in a continuum elastic space[42,43]. In the rigid block motion model, any spot on a block is considered to rotate around an axis, which passes through the center of the Earth, at the same angular rate, and fault slip is considered as the result of relative block motion along boundaries. Therefore, fault slip rates are not independent of each other, but have to meet the requirements of kinematic consistency and continuity. This means that the slip rate of each fault is dependent on the relative angular rotation rate between the two blocks separated by the fault, thus the slip rates of adjacent faults on their intersection point should observe deformation continuity. In reality, the crust is not completely rigid, so regional variations of deformation exist in space and time, and deformation continuity at the intersection points of linked faults does not always hold. In contrast to the block motion model, the fault dislocation model usually simulates displacements at the Earth's surface by summing up the contributions from slip on individual fault segments, neglecting the intrinsic correlation and interaction of neighboring faults. In the case of weak data constraints, to fit the regional deformation data, the model often yields unreasonable results such as large differences between slip rates and/or even opposite motions of adjacent fault segments. A priori constraints in such cases are usually needed.

In order to better simulate the deformation field, we employ a linked-fault-element model developed by Zeng and Shen[44]. This model is based on the Okada fault dislocation model, but imposes finite constraints on slip rates of adjacent fault elements. The model corresponds to two end-member models in two extreme cases: when very strict constraints are imposed, it equals the block motion model; but when no constraints are imposed, it returns back to the fault dislocation model. By imposing appropriate constraints, we can reasonably model the surface deformation field, so that the overall continuity of deformation is enforced to certain extent, and limited regional variations of deformation in the neighborhood of adjacent faults are also allowed.

The relationship between the GPS velocity observables and the fault slip rates is:

$$\boldsymbol{y}=\boldsymbol{A}\boldsymbol{x}+\boldsymbol{e}, \tag{1}$$

where $\boldsymbol{y}$ is the velocity data vector composed of the eastward and northward velocity components of GPS stations, $\boldsymbol{x}$ is the fault slip rate vector composed of the strike-slip and normal components of the faults, and $\boldsymbol{A}$ is the mapping matrix linking individual observables to the model parameters. $\boldsymbol{e}$ is the error vector following the normal distribution $\boldsymbol{e}\sim N(0, \boldsymbol{C})$, where $\boldsymbol{C}$ is the variance/covariance matrix of the velocity data errors.

The continuity constraints on the intersection points of linked elements and the constraints on fault normal components are added:

$$0=\boldsymbol{B}\boldsymbol{x}+\boldsymbol{s}, \tag{2}$$

where $\boldsymbol{B}$ is the mapping matrix composed of the continuity constraints on the intersection points of linked elements and the constraints on fault normal components. $\boldsymbol{s}$ is the corresponding error vector following the normal distribution $\boldsymbol{s}\sim N(0, \boldsymbol{D})$. Under the strict continuity con-

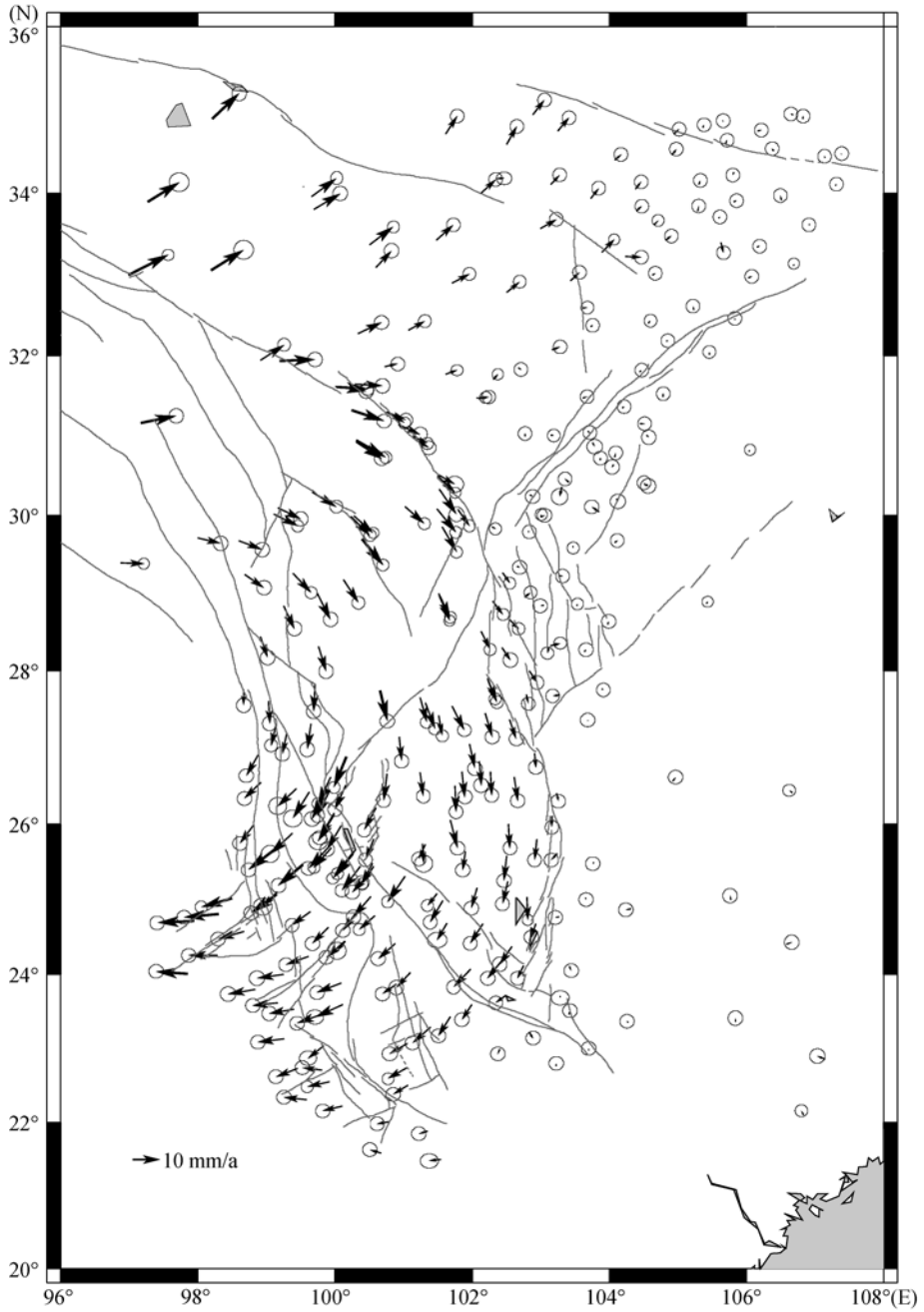

Figure 2 GPS velocity field of the Sichuan-Yunnan region with respect to the South China block. The error ellipses represent 70% confidence.

straints, 0=$\boldsymbol{Bx}$. The covariance matrix $\boldsymbol{D}$ helps introduce errors into the continuity constraints of fault slip on intersection points of linked elements and constraints on fault normal components. $\boldsymbol{D}$ is a diagonal matrix. The square roots of its diagonal terms constitute a vector $\boldsymbol{d}$, corresponding to the uncertainties of the kinematic constraints. An element of $\boldsymbol{d}$ for introducing error to the fault slip rate continuity on an intersection point is defined as

$$d_c=\sqrt{\frac{n}{F\cdot D_c^2}}, \tag{3}$$

where n is the number of faults intersecting at the point. $F=\sum_i^n \frac{4}{L_i^2}$, L_i is the length of the i-th fault at the point. D_c is a parameter to be determined for adjusting the constraint on the dislocation continuity. The more the faults are intersecting at one point with longer length, the more

the more the real data are involved in constraining the solution of the slip rates, therefore, higher resolutions of the results will be obtained for the slip rates, and the constraints can be relaxed more. Also, the more the faults are intersecting at one point, the more likely the fault slip rates become discontinuous, leading to allowance of higher a priori uncertainties of the continuity constraints. In summary, the constraint is dependent on the value of d_c. When d_c=0, the continuity constraint on fault slip is completely satisfied, corresponding to the rigid block motion model, and when d_c goes to infinity, the fault slips are completely independent of each other, corresponding to the Okada fault dislocation model. The larger the D_c is, the smaller the d_c will become, and the tighter constraint is imposed on fault slip.

Furthermore, if not properly constrained, unreasonably large normal components may be obtained on some strike-slip faults not well constrained by data, due to the uneven spatial distribution of the GPS network. To avoid such situation, we introduce an element d_n as the component of vector $\boldsymbol{d}$, to constrain the normal component of a fault. d_n is defined as

$$d_n=1+\frac{L_i}{D_n}, \tag{4}$$

where D_n is a parameter for adjusting the constraint on the normal component of the fault. Similarly, the greater length the fault has, the more the data are involved in constraining the model parameters, and the constraint on the normal component is more relaxed.

Combining eqs. (1) and (2), we have the set of equations linking fault slip rates with the GPS station velocities under the a priori constraints:

$$\begin{bmatrix} \boldsymbol{y} \\ 0 \end{bmatrix} = \begin{bmatrix} \boldsymbol{A} \\ \boldsymbol{B} \end{bmatrix} \boldsymbol{x} + \begin{bmatrix} \boldsymbol{e} \\ \boldsymbol{s} \end{bmatrix}. \tag{5}$$

The solution can be obtained using the least squares method in the form of

$$\boldsymbol{x} = [\boldsymbol{A}^T \boldsymbol{C}^{-1} \boldsymbol{A} + \boldsymbol{B}^T \boldsymbol{D}^{-1} \boldsymbol{B}]^{-1} \boldsymbol{A}^T \boldsymbol{C}^{-1} \boldsymbol{y}. \tag{6}$$

The postfit residuals reflect the fitting of GPS data to the model, providing a basis for filtering data and adjusting the fault geometry. If large velocity residuals in a local area are biased to one direction, the fault model should be modified, by either adding new fault elements or altering the geometry of some fault elements to follow different geological fault traces, in order to fit the GPS velocity field better. Through multiple iterations of trial-and-error, large postfit residuals have generally been removed.

The resolution matrix of the results is defined as

$$\boldsymbol{R}=[\boldsymbol{A}^T \boldsymbol{C}^{-1} \boldsymbol{A} + \boldsymbol{B}^T \boldsymbol{D}^{-1} \boldsymbol{B}]^{-1} [\boldsymbol{A}^T \boldsymbol{C}^{-1} \boldsymbol{A}], \tag{7}$$

whose diagonal elements are the resolutions of model parameters, representing the weights of real data in the final solution[45,46]. In fact, because of the a priori constraints on the continuity and normal components of fault slip, only fractions of the final solutions are constrained by the real data. Generally speaking, regions with dense GPS station coverage, data with small errors, or faults with long patches often result in high resolution of slip rates. Low resolutions often occur in areas with short fault patches, reflecting strong dependence of results on how the fault patches are divided in the model. Nevertheless, low resolutions do not always mean low confidence. In some cases, a fault is divided into small patches in order to accommodate its large curvature; if it is to evaluate the combined effect of two or more linked fault patches, one should examine the weighted average of these fault patches, and check the sum of their individual resolutions, which may not be low.

4 Results

Our initial model is constructed based on knowledge from previous studies, such as the block boundaries in the Sichuan-Yunnan region[36], main active faults in continental China[47], and the late Cenozoic to Holocene tectonics in the Sichuan-Yunnan region[48] (Figure 1). Since the vertical components of the GPS velocities are much less reliable than the horizontal components, only the horizontal velocity data are used in the inversion. In the fault model, we assume a uniform 90° dip angle for all the fault elements, because: (1) information about fault dip angles is scarce and not reliable in general; (2) the complexity of fault geometry cannot be solely accounted for by dip angle only, and introduction of dig angle into the parameters may not improve the solution much but bring additional uncertainties into the model. Therefore, dip angles of all faults are constrained to be 90°, allowing only the strike-slip and normal components across the faults. The thrust or normal faulting effect across an inclined fault in reality is represented by the horizontal normal components. Such an approximation is able to reasonably simulate the far-field deformation induced by the dislocation of inclined faults, while ignoring the asymmetry of near-field deformation. Provided that the GPS data used in the modeling are mostly far-field with respect to the fault patches studied for

most cases, errors introduced by the approximation should be rather limited. Such practice has been successfully applied in some previous studies, such as the ones by Meade and Hager[49] and McCaffrey[50]. Based on the hypocenter location results of small earthquakes[51] we determine the fault locking depths as the depths separating 95% of the small earthquakes occurred above from 5% below. But this approach is not suitable for regions with low seismicity or sparse seismic station coverage. In these cases, we determine the fault locking depths based on the regional average depths or the fault types. For some important faults constrained by abundant data, we repeatedly examine the data postfit residuals and modify the fault locking depths until the best data fitting is achieved (Figures 3 and 4, Table 1).

The inversion results of the strike-slip components

Table 1 Modeling results of fault slip rates[a)]

Fault	Strike-slip component			Normal component		
	Amplitude ($mm \cdot a^{-1}$)	Uncertainty ($mm \cdot a^{-1}$)	Resolution	Amplitude ($mm \cdot a^{-1}$)	Uncertainty ($mm \cdot a^{-1}$)	Resolution
NW segment of Garzê-Yushu fault	–3.1	2.8	0.44	–2.8	2.7	0.51
SE segment of Garzê-Yushu fault	–13.0	1.7	0.34	7.4	1.4	0.25
Garzê-Luhuo segment of Xianshuihe fault	–13.4	1.5	0.18	7.8	1.2	0.25
Luhuo-Daofu segment of Xianshuihe fault	–15.7	1.4	0.14	0.1	1.2	0.22
Daofu-Kangding segment of Xianshuihe fault	–15.6	1.4	0.23	–2.7	1.1	0.39
Kangding-Shimian segment of Xianshuihe fault	–11.2	2.3	0.24	2.5	2.0	0.29
Anninghe fault	–5.1	2.5	0.11	–0.1	2.4	0.06
Zemuhe fault	–2.8	2.3	0.46	3.8	1.9	0.51
Daliangshan fault	–7.1	2.1	0.45	0.4	1.8	0.47
Xiaojiang fault	–9.4	1.2	0.52	1.5	1.0	0.58
Southwest extension of Xiaojiang fault	–10.1	2.0	0.13	–2.2	2.4	0.21
Daluo-Jinghong fault	–7.3	2.6	0.45	1.1	1.6	0.33
Mae Chan fault	–4.9	3.0	0.49	–0.5	2.2	0.31
NW segment of Red River fault	0.4	1.6	0.34	–1.5	1.3	0.30
Central segment of Red River fault	0.3	1.3	0.67	1.0	1.5	0.75
SE segment of Red River fault	–1.5	2.7	0.34	–1.3	2.0	0.25
Nanhua-Chuxiong-Jianshui fault	4.2	1.3	0.81	0.9	1.2	1.09
North Lancang River fault segment north of Bitu	–5.1	2.1	0.57	5.2	2.3	0.56
North Lancang River fault segment south of Bitu	2.4	1.2	0.16	0.8	1.1	0.15
Baiyu fault	–0.4	1.9	0.44	4.0	1.9	0.42
Weixi-Weishan fault	1.3	1.0	0.60	1.5	1.1	0.64
Wuliangshan fault	4.3	1.1	0.38	0.6	1.1	0.59
Nujiang fault	0.3	2.3	0.47	–0.3	2.7	0.28
Longling-Lancang fault	8.5	1.7	0.37	0.1	1.6	0.53
Litang fault	–4.4	1.3	0.61	2.7	1.1	0.86
Longriba fault	5.1	1.2	0.87	0.8	1.1	1.13
Baoxing-Beichuan segment of Longmenshan fault	0.2	1.0	0.45	–1.4	1.0	0.62
Beichuan-Qingchuan segment of Longmenshan fault	–1.0	1.2	0.13	–1.6	1.3	0.14
Qingchuan-Nanzheng segment of Longmenshan fault	–1.5	1.3	0.53	–2.9	1.4	0.53
Deyucuo-Yinmahu fault	0.3	2.1	0.79	–2.8	1.6	0.89
NE segment of Lijiang-Xiaojinhe fault	–0.8	1.5	0.27	2.4	1.7	0.30
Central segment of Lijiang-Xiaojinhe fault	–5.4	1.2	0.22	–0.5	1.0	0.28
SW segment of Lijiang-Xiaojinhe fault	–0.5	1.6	0.21	–2.3	1.8	0.24
Batang fault	8.7	2.1	0.34	1.1	1.9	0.28
Yunongxi fault	2.7	2.3	0.56	–6.7	2.3	0.64
Yingjing-Mabian-Yanjin fault	–1.2	1.2	0.49	–2.1	1.4	0.81
Daying River fault	0.9	3.0	0.19	–7.8	2.8	0.31
Longling-Ruili fault	–3.1	2.4	0.43	0.4	2.0	0.32
Nantinghe fault	–4.3	1.6	0.62	1.2	1.5	0.82
Kunlun fault	–7.1	1.4	0.99	–3.5	1.5	1.13

a) Positive for right-lateral and extension.

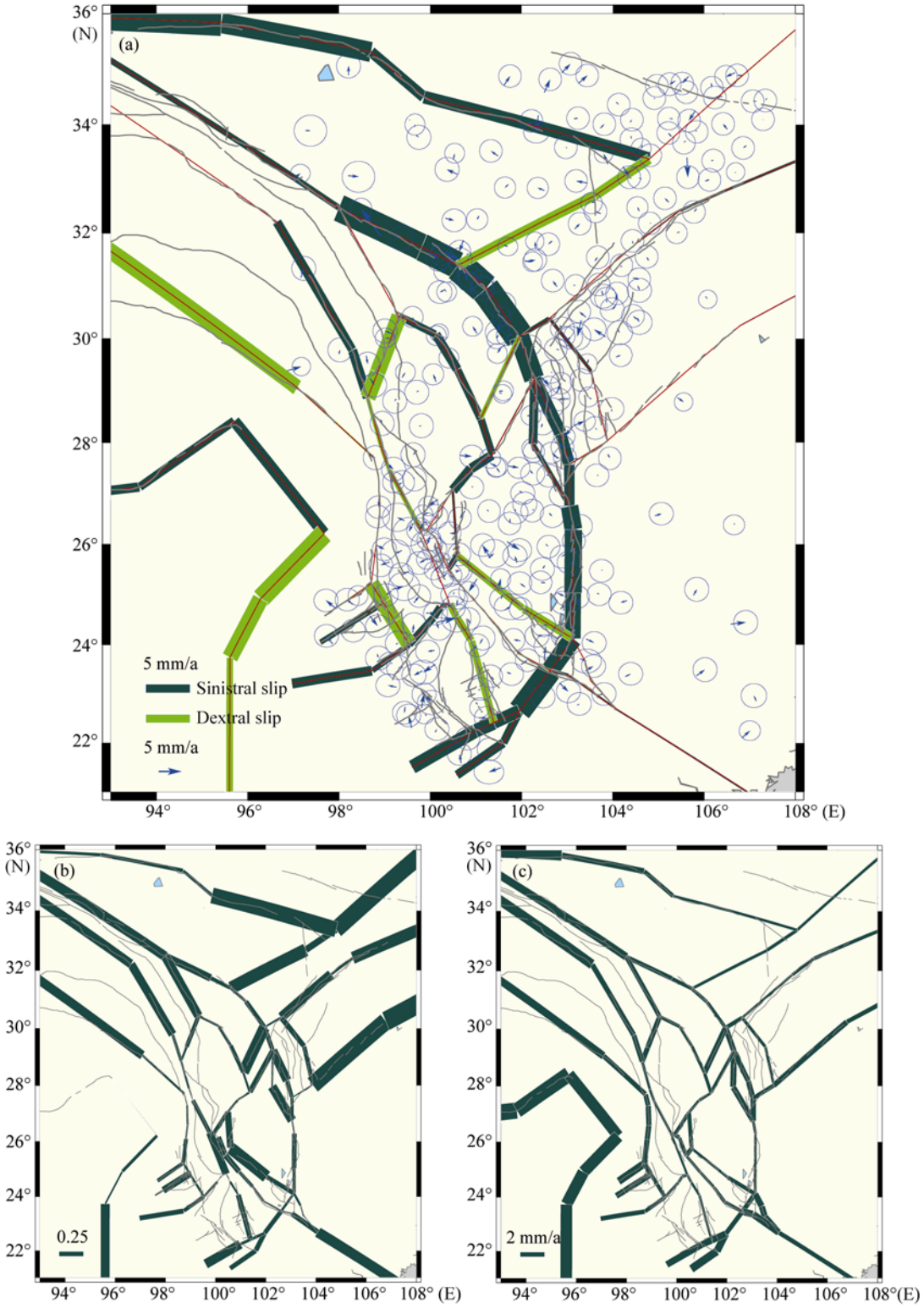

Figure 3 Results of strike-slip components in Sichuan-Yunnan region. (a) Slip rate; (b) resolution; (c) uncertainty.

show that the most active fault zone is characterized by left-lateral strike-slip. It stretches from the Garzê-Yushu fault in the northwest, passes through the Xianshuihe fault, splays into the Anninghe-Zemuhe and Daliangshan faults, converges southward into the Xiaojiang fault, and transpasses the central segment of the Red River fault to extend southwestward. The faults located west of the Sichuan-Yunnan block are characterized mainly by

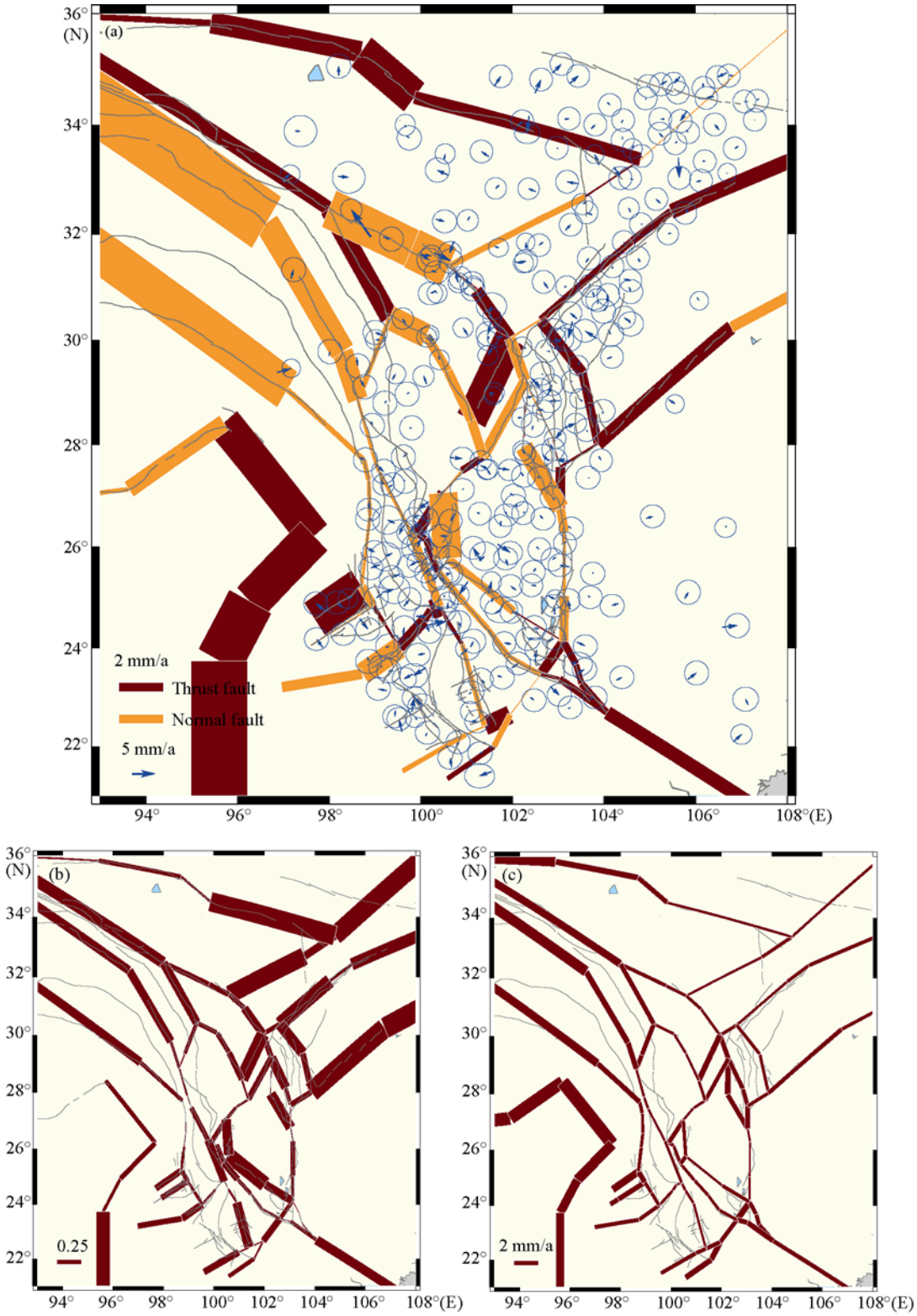

Figure 4 Results of normal components in Sichuan-Yunnan region. (a) Slip rate; (b) resolution; (c) uncertainty.

right-lateral strike-slip. Also, the inversion results indicate that most of the N-S or NW-SE trending faults have an extensional component, while most of the NE-SW trending faults have a compressional component. More detailed analysis of the inversion results is given in the following sections.

4.1 Xianshuihe-Xiaojiang fault zone

This is the most active large-scale fault system in the region, characterized by left-lateral strike-slip motion, and composed of the Garzê-Yushu, Xianshuihe, Anninghe, Zemuhe, Daliangshan, Xiaojiang faults, the segment across the Red River fault, and the Daluo-Jinghong and Mae Chan faults. The strike-slip rates across the NW and SE sections of the Garzê-Yushu fault are 3.1±2.8 and 13.0±1.7 mm/a, respectively. The slip rate of the SE section of the Garzê-Yushu fault is consistent with the average slip rate of 12±2 mm/a over the past 50 ka estimated by Wen et al.[13] from geomorphic offsets and ages of related sediments, and also with that of 14±3 mm/a reported by Xu et al.[14].

Shen et al.[52] derived a strain rate field of continental China using GPS data, and pointed out that next to the Himalayas, the Xianshuihe fault region has the second highest strain rate in continental China. Shen et al.[36] determined the left-lateral slip across the Xianshuihe fault at a rate of 10－11 mm/a by projecting the GPS velocity onto the strike of the fault. Sun et al.[4] estimated the shear strain rate across the fault zone as 10.9 mm/a through seismic moment inversion. Our inversion results reveal that the Xianshuihe fault slips left-laterally at a rate of 8.9－17.1 mm/a, and the slip rate increases first and then decreases from NW to SE, which is consistent with but slightly higher than previous results[2−5,8−10,14,17,35,36]. Significant extensions appear across the SE section of the Garzê-Yushu fault and the Garzê-Luhuo section of the Xianshuihe fault, possibly associated with a pull-apart basin created by a right step between these two left-slip faults. However, the amount of left slip is not large enough to produce such a large extension across the faults. Since the resolutions of the normal components are 0.25 for both of the fault sections, the results do not seem to be quite reliable, possibly resulting mainly from the continuity constraints associated with the adjacent faults.

The Xianshuihe fault splays at Shimian into two branches: the Anninghe-Zemuhe and Daliangshan faults, both characterized by left slip. We determine the slip across the Anninghe and Daliangshan faults at rates of 5.1±2.5 and 7.1±2.1 mm/a, respectively, with the amplitudes of their slip decreasing southward. The strike-slip rate of the Anninghe fault is consistent with that reported by Zhou et al.[10] (4.7－5.3 mm/a), Xu et al.[14] (6.5±1.0 mm/a), and Shen et al.[36] (4±2 mm/a), but quite different from that reported by Shen et al.[8] (30 mm/a left slip and 9－11 mm/a extension). The strike-slip rate of the Daliangshan fault is larger than that reported by Xu et al.[14] (3.3±0.7 mm/a). The strike-slip rate of the Zemuhe fault (2.8±2.3 mm/a) is smaller than that reported by Xu et al.[14] (6.4±0.6 mm/a) and that reported by Shen et al.[36] (7±2 mm/a). Han and Jiang[53] revealed that the frequency of the moderate and strong earthquakes in the Anninghe-Zemuhe seismic belt was higher than that in the Daliangshan seismic belt. They concluded that across the former the average fault slip rate was larger and the average recurrence time interval of strong earthquakes was shorter than that across the latter, suggesting more release of seismic strains along the Anninghe-Zemuhe fault during the past centuries. Significant amount of elastic strains therefore might have been accumulating along the Daliangshan fault, increasing its earthquake risk. However, less research has been conducted on the Daliangshan fault than that on the Anninghe fault, and their conclusions might be biased by the incomplete collection of the data. The 3.8±1.9 mm/a extension across the Zemuhe fault is likely the result of a right step between the left slip Anninghe and Xiaojiang faults.

The Zemuhe and Daliangshan faults extend southward into the Xiaojiang fault, which then splays into two branches. Limited by the station coverage in the region, the total slip rate of the two branches, rather than their individual slip rates, is estimated. The 9.4±1.2 mm/a left slip of the Xiaojiang fault is consistent with the 10±2 mm/a estimate of Song et al.[6] and the 13.0－16.5 mm/a slip of He et al.[12], and slightly larger than the 7±2 mm/a slip reported by Shen et al.[36].

Shen et al.[36] detected 7±2 mm/a left slip across the southwestward continuation of the Xiaojiang fault which extends across the Red River fault. Our results also reveal an NE trending deformation zone with a slip rate of 10.1±2.0 mm/a, larger than that reported by Shen et al.[36]. This deformation zone extends southwestward and connects with the Daluo-Jinghong and Mae Chan faults, which slip left-laterally at rates of 7.3±2.6 and 4.9±3.0 mm/a, respectively. The Garzê-Yushu, Xianshuihe, Anninghe, Zemuhe, Daliangshan, and Xiaojiang faults, the deformation zone cross Red River fault, and the Daluo-Jinghong and Mae Chan faults constitute the northeastern and eastern boundaries of the eastward

extrusion of the southeast Tibetan Plateau.

4.2 Jinsha River-Red River fault zone

Previous studies revealed some activities of the Dêqên-Zhongdian-Daju and Jinsha River faults[11,16,18]. But our modeling result yields small velocity postfit residuals in the region without deploying corresponding fault patches in the model, implying little recent fault activities across these faults. The Red River fault is a large-scale structure slicing the entire lithosphere; together with the Jinsha River fault, it was regarded as the southwestern boundary of the Sichuan-Yunnan block. Previous studies suggested that the fault had been active since late Pleistocene. Nevertheless, our result yields merely modest faulting rates, 0.4±1.6 mm/a right slip and 1.5±1.3 mm/a shortening across its NW section, 0.3±1.3 mm/a right slip and 1.0±1.5 mm/a extension across its central section, and 1.5±2.7 mm/a left slip and 1.3±2.0 mm/a shortening across its SE section respectively, approximately consistent with the previous results[36,54,55]. In fact, the seismicity pattern indicates no obvious activity across the Red River fault in recent years. Instead, the Nanhua-Chuxiong-Jianshui fault and the Wuliangshan fault, located NE and SW of the Red River fault respectively, show right slip at rates of 4.2±1.3 and 4.3±1.1 mm/a, respectively. All the results described above support the inference of Wang et al.[15] that the southwestern boundary of the eastward extrusion of the Tibetan Plateau is composed of a group of distributed dextral faults slipping at low rates.

4.3 Lancang River-Weixi-Weishan-Wuliangshan fault zone

This is another arch-shaped fault system in the studied region. No corresponding fault patches are set for the South Lancang River fault in our model (Figure 1). Compared to the Xianshuihe-Xiaojiang fault system, this fault system has much slower slip rates. The segment of the North Lancang River fault north of Bitu slips left-laterally at a rate of 5.1±2.1 mm/a and extends at a rate of 5.2±2.3 mm/a. The right slip and extension rates for the segment south of Bitu are 2.4±1.2 and 0.8±1.1 mm/a, respectively. The resolution of the strike-slip component for the segment north of Bitu is 0.57, suggesting that the result is credible to some extent. But the south segment is loosely constrained by data with its resolution of only 0.16, being not quite reliable. Furthermore, the 5.2±2.3 mm/a extension across the segment of the North Lancang River fault north of Bitu and the 4.0±1.9 mm/a shortening across the Baiyu fault may not be real but the result of negative correlation between the two fault segments, since there is a lack of GPS stations in the region between the two faults. The Wuliangshan fault slips right laterally at a rate of 4.3±1.1 mm/a. What should be pointed out is that the GPS data used in this study were observed from 1994 to 2006. The *Ms* 6.4 Pu'er earthquake occurred in July 2007 along the Wuliangshan fault zone, verifying that it is indeed an active fault at present.

4.4 Nujiang-Longling-Lancang fault zone

Only 0.3±2.3 mm/a right slip is detected across the Nujiang fault. The Longling-Lancang fault, located south of the Nujiang fault (corresponding to the Shidian deformation zone reported by Shen et al.[36]), slips right laterally at a rate of 8.5±1.7 mm/a, consistent with a ~6 mm/a right-lateral shear reported by Shen et al.[36] Results from magnetotelluric exploration[56], active tectonics[7], and GPS surveys[35,36] all indicate the existence of a new fault zone in the region.

4.5 Litang fault

Our results reveal 4.4±1.3 mm/a left slip and 2.7±1.1 mm/a extension across the Litang fault. Its strike-slip rate is consistent with the 4±1 mm/a slip reported by Xu et al.[14,18] and the 2.6—4.4 mm/a slip reported by Zhou et al.[57] On the other hand, the extension rate obtained is slightly different from the 0.1—1.8 mm/a estimate reported by Xu et al.[18], but consistent with the average extensional strain rate of $(13.6\pm2.0)\times10^{-9}$ a^{-1} determined by Gan et al.[37].

4.6 Faults in Longmen Mountains region

Recent studies indicate that there are no significant tectonic activities around the Longmen Mountains, across which the shortening rate must be lower than 3.0 mm/a[17,36]. Burchfiel[58] hypothesized that driven by the gravitational potential from the central Tibetan Plateau, the materials in the lower crust flow eastward, elevating the topography of the eastern borderland of the Tibetan Plateau. The steep Longmen Mountain frontals were created by the sharp contrast between the lower crust rheologies of the eastern plateau and the Sichuan Basin. The lack of ductile lower crust in the Sichuan Basin blocked the eastward crustal flow from the eastern plateau, resulting in thickening of the crust and elevating

the Longmen Mountains. This interpretation is consistent with the observation that the Longmen Mountain front and its vicinity had little shortening during the late Cenozoic. Our results depict 1.4±1.0 and 1.6±1.3 mm/a shortening across the Baoxing-Beichuan and Beichuan-Qingchuan segments, and 1.5±1.3 mm/a sinistral slip and 2.9±1.4 mm/a shortening across the Qingchuan-Nanzheng segment. Although high resolutions are obtained for both slip components of the Qingchuan-Nanzheng segment, reliabilities of the slip rates are to be examined however, since tradeoff may exist between the Qingchuan-Nanzheng segment and the faults south of it, and the NE extension of the segment to the far field does not follow precisely the trace of any known fault. Right lateral slip has been detected across a deformation zone, and recognized recently as the Longriba fault (Wen X Z, private communication, 2007), NW of the Longmen Mountains at a rate of 5.1±1.2 mm/a, which is consistent with the 2—8 mm/a slip reported by Shen et al.[36] At the same time, 2.8±1.6 mm/a shortening is found across the Deyucuo-Yinmahu fault located southeast of the Longmen Mountains. This may be interpreted as the result of slip partitioning, often observed along plate boundaries undergoing oblique subduction.

4.7 Lijiang-Xiaojinhe fault zone

This fault zone is a sub-block boundary within the Sichuan-Yunnan block. It is separated into three segments. The NE segment is transtensional with modest amount of slip: 0.8±1.5 mm/a left slip and 2.4±1.7 mm/a extension. The central segment is characterized by left lateral slip at a rate of 5.4±1.2 mm/a. The SW segment is mainly converging, with a shortening rate of 2.3±1.8 mm/a. Shen et al.[36] estimated the left slip rate of the Lijiang-Xiaojinhe fault as 3 mm/a. Gan et al.[37] detected an abrupt change of strain pattern across the fault. Xu et al.[14] determined its geological left slip and shortening rates to be 3.8±0.7 and 0.6±0.1 mm/a, respectively. Based on analysis of synsedimentary dislocation of the basins and age determination, Xiang et al.[59] measured the average slip rate over the Holocene time as 2.5—5.0 mm/a. The above studies revealed the important role of this fault played in crustal deformation of the Sichuan-Yunnan region.

4.8 Batang fault

Batang fault has been active in late Quaternary, evidenced by the 1970 *Ms* 7 Batang earthquake. Zhou et al.[57] measured its right slip rate to be 1.3—2.7 mm/a by interpreting the TM satellite images and aerial photographs. We derive a higher right slip rate of 8.7±2.1 mm/a and 1.1±1.9 mm/a extension across the fault. But the resolutions of this fault are relatively low, with total resolutions of the strike-slip and extensional components being 0.34 and 0.28, respectively. The results, to a great degree, come from the continuity constraints associated with the adjacent faults, instead of GPS data in the region.

4.9 Yunongxi fault

The Yunongxi fault is the western boundary of the Gongga Mountain block which has been uplifting in the Holocene time. The 1975 *Ms*6.2 Kangding earthquake occurred along this fault. Based on its dislocation morphology Huang et al.[60] concluded that it was a weakly active Holocene fault, with an average thrust rate of 0.5—0.6 mm/a. Based on dislocation measurements of gullies and river terraces, C^{14} dating data, and estimates of sediment age, Chen[61] estimated its left slip and thrust rates as 3 and 1 mm/a, respectively. Our results suggest strong contemporary activity along this fault, with a right slip rate of 2.7±2.3 mm/a and a shortening rate of 6.7±2.3 mm/a, higher than previous results. However, our results seem to be consistent with the result obtained by Wang (Wang Q L, Private communication, 2007): Based on leveling data surveyed from 1973 to 2006, an uplifting rate detected for a region near the Gongga Mountain is > 4.0 mm/a with respect to Ya'an, and > 5.7 mm/a with respect to Yibin. Since the crustal material is almost incompressible, the vertical uplift often implies thickening of the crust or horizontal shortening. The leveling data revealed the rising trend of the Gongga Mountain and its surrounding areas. The associated horizontal deformation in this region is probably distributed in the regional crust, instead of concentrating along faults. Our results could be interpreted as the crustal shortening in the region around the Yunongxi fault, resulting from the lateral resistance to the southeastward motion of the crustal material in the Gongga Mountain region, causing the regional compression and uplifting of the Gongga Mountain. Limited by the station density in the region, we provide a regional crustal shortening rate rather than unambiguous estimate of the slip across the Yunongxi fault.

4.10 Faults around the eastern Himalayan syntaxis

Faults around the eastern Himalayan syntaxis are separated into three segments. Faults west, NE, and SE of the syntaxis are characterized by left-lateral transtension, left-lateral transpression, and right-lateral transpression, respectively. Since these faults are not constrained by GPS data, the results are unreliable. Nevertheless, the approximate boundary conditions provided by these faults are indispensable for the modeling work of this study.

5 Discussion

5.1 Impacts of continuity and normal component constraints

It is considered that on one hand, proper a priori constraints in the model can fill in the gap left by the insufficient amount of data and balance the regional deformation field; on the other hand, however, too strong a priori constraints can bias the model result, diminish the weight of data on the result, and reduce the model resolution. Therefore, proper constraints are needed for the rationality and susceptibility of the model. Besides the constraints associated with geometries of the fault system, the continuity constraint parameter D_c and the normal component constraint parameter D_n are quite important in the inversion. We can obtain the optimal values of these parameters by balancing a trade-off between the postfit residual χ^2 and the total resolution through a series of trials, so that the data will be reasonably interpreted and the results will be properly constrained simultaneously[46].

Maintaining a fixed ratio between D_c and D_n at 2∶1, we vary them from (0, 0) km (corresponding to the first point from right, the loosest constraints on the model) to (5000, 2500) km (corresponding to the first point from left, the strongest constraints on the model), and the trade-off line between the postfit residual χ^2 and resolution is plotted in Figure 5. As the postfit residual χ^2 decreases along with the increase of the resolution, the fitting of the model to the data gets better, and the constraints on the model become looser. As the results become more dependent on the data, the data can be over-interpreted, i.e. significant amount of data errors may be mapped into the results. Notice that the postfit residual χ^2 is reduced less as the resolution increases. The trade-off curve was separated into two segments by a turning point at which the normalized slope is –1. We select the corresponding values of the parameters (D_c=50 km, D_n=25 km) on the spot to constrain the model, with a corresponding total resolution of 48.38.

5.2 Impacts of locking depths

GPS data are more densely distributed around the Xianshuihe and Xiaojiang faults, and have good constraints on the results of fault locking depths. Therefore, we select the segments of the Xianshuihe and Xiaojiang faults, vary their locking depths and calculate the postfit residual χ^2. Figure 6 shows the data fitting curve, postfit residual χ^2 versus the fault locking depth. The optimal value of locking depth corresponds to the minimum of the postfit residual χ^2. The optimal locking depths of the Xianshuihe and Xiaojiang faults are 15 and 17 km, respectively, with 70% confidence ranges of 11－19 km and 11－25 km, estimated using the F-test. Locking depths of other faults could not be well estimated, since the faults are not large enough, and there are no sufficient data in the neighboring regions to constrain the model parameters, or it is difficult to differentiate the interaction from adjacent fault patches.

5.3 Comparison between linked-fault-element approach and profile projection method

Fault slip rates inverted from the linked-fault-element approach are generally higher than those estimated by the profile projection method. The cause ought to be the difference between the two methods. The profile projection method estimates fault slip rates by leveling the far-field velocity data, assuming the deformation field across the faults to be one dimensional. Since the results are obtained based on the large-scale deformation field, they tend to be stable. However, since the deformation field is often two-dimensional other than one-dimensional, especially at the near-field, ignoring the two-dimensional deformation signals often leads to failure of adequately modeling slip variation along faults. In addition, slip amount will be underestimated when the fault is not long enough to satisfy the assumption that the far-field deformation is produced by dislocation of infinitely long fault. Without such an assumption, the linked-fault-element approach is better at estimating the variation of slip rate along faults. The minus side of the approach is that when there is a lack of data or the faults are divided into too small patches, the result may become unstable if not properly constrained. Differences

between the two approaches explain why our results on the Xianshuihe fault are higher than those of Shen et al.[36]. Through examining the GPS data distribution in the vicinity of the Xianshuihe fault, our fault model geometry, and the resolutions of fault elements shown in Figure 3(b), we believe that although the inverted result of a single fault element may not be so reliable, the overall estimate of 8.9—17.1 mm/a slip obtained from stacking several linked fault patches together should be reliable. The slip rate obtained from GPS is slightly higher than that from geology, which may result from the difference in time coverages of the GPS and geologic observations used to derive the mean slip rates.

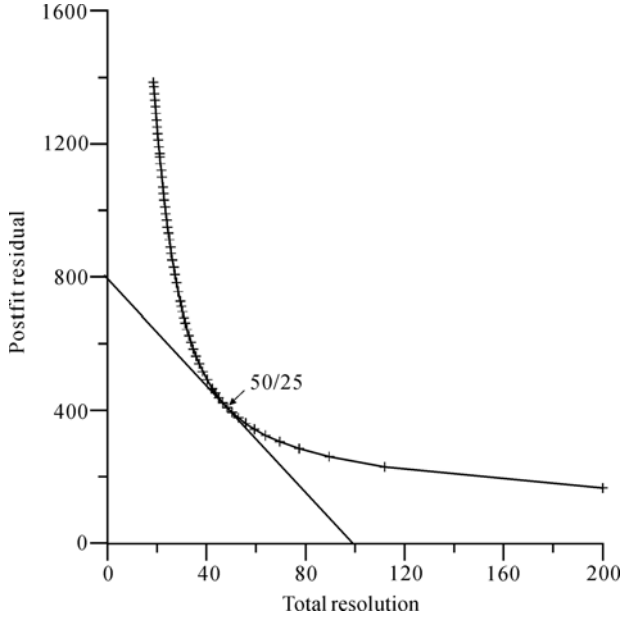

Figure 5 Relationship between total resolution and postfit residual with the increase of D_c. The corresponding values of the arrow-directed point are used in the model.

5.4 Limitation of our model in complex fault systems

There are several regions crosscut by two groups of conjugate faults. One is the Yingjing-Mabian-Yanjin fault zone, an important NW-trending seismic belt at the southeastern margin of the Tibetan Plateau, composed of two groups of conjugate faults. Two large earthquakes of $M > 7$ and many strong earthquakes of $M6—6.75$ have occurred in this region[62]. Limited by the distribution of GPS stations, only two NW-trending fault patches are included in our model, and the horizontal shortening rate across the fault zone is estimated as 2.1±1.4 mm/a. The Dayingjiang, Longling-Ruili, and Nantinghe faults are all NE-trending faults crosscutting the Nujiang fault. Due to the lack of data outside the China border, our fault model has the extents of these faults limited inside the borderline. In real world, they are likely to extend beyond. With the far-field integrating effect ignored, our inverted results might be higher than those in reality. We find a large shortening rate across the Dayingjiang fault, and large left-lateral slip rates across the Longling-Ruili and Nantinghe faults. There are also conjugated faults in the Simao-Pu'er region, but only one NW-trending fault is defined in the model, which yields a high dextral slip rate. All the regions mentioned above have strong seismicity, but no fine image of crustal deformation has been resolved from the GPS velocity field yet, because of the limitation of GPS station distribution there.

6 Conclusions

Slip rates of main faults in the Sichuan-Yunnan region are inverted by applying the linked-fault-element approach constrained using GPS velocity field. Our results

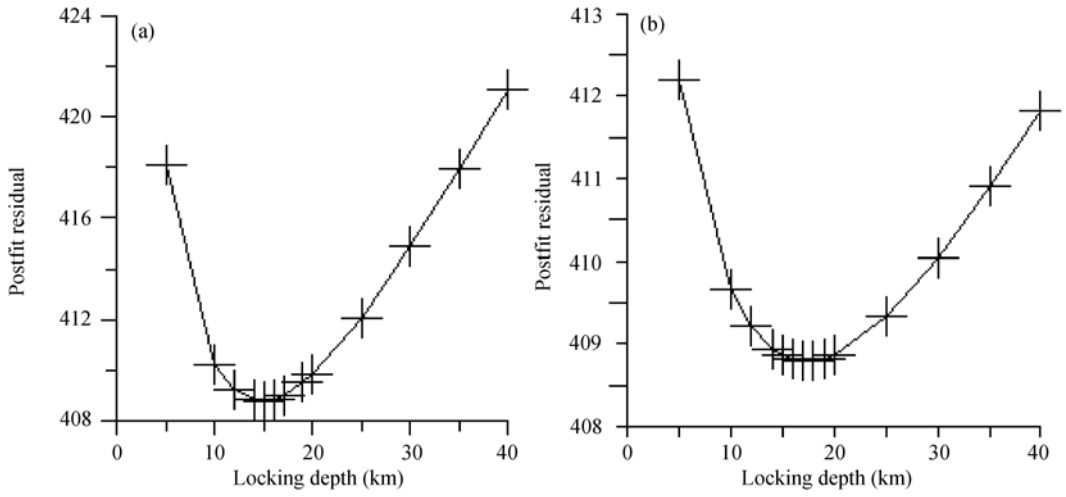

Figure 6 Relationship between postfit residual χ^2 and locking depth. (a) Xianshuihe fault; (b) Xiaojiang fault.

reveal that the Xianshuihe-Xiaojiang fault zone is the largest-scale fault system in the region, and behaves as the northeast and east boundaries of the materials extruded eastward from the eastern Tibetan Plateau. The slip rates of the Garzê-Yushu, Xianshuihe, Anninghe, Zemuhe, Daliangshan, and Xiaojiang faults, the southwest extension of the Xiaojiang fault across the Red River fault, and the Daluo-Jinghong and Mae Chan faults are determined to be 0.3 — 14.7, 8.9 — 17.1, 5.1±2.5, 2.8±2.3, 7.1±2.1, 9.4±1.2, 10.1±2.0, 7.3±2.6, and 4.9±3.0 mm/a, respectively. Within the Garzê-Yushu fault, the left-slip rates are 3.1±2.8 and 13.0±1.7 mm/a for the NW and SE segments. Within the Xianshuihe fault, the left-slip rates are 13.4±1.5, 15.7±1.4, 15.6±1.4, and 11.2±2.3 mm/a for the Garzê-Luhuo, Luhuo-Daofu, Daofu-Kangding, and Kangding-Shimian segments respectively. The abundant slow slipping faults described above are in direct contradiction with the "block motion" model which hypothesized that continental escape was realized by fast slip along a rather limited number of large scale strike-slip faults.

The western boundary of the material flow is not clear, but behaves as a broad right-lateral shear deformation zone whose activity is weaker than that of the Xianshuihe-Xiaojiang fault zone. No significant strike slip components are found across the Red River fault, which previously was considered as a major transform fault within the continental plate. Significant deformation is detected across the Nanhua-Chuxiong-Jianshui and Wuliangshan faults on both sides of the Red River fault.

Our results of the Longmenshan and Longriba faults support previous understanding[36] that there is only weak tectonic activity in the Longmen Mountains region, with shortening rates of 1.4±1.0 and 1.6±1.3 mm/a across the Baoxing-Beichuan and Beichuan-Qingchuan segments, and there is a significant right-lateral slip across the Longriba fault zone with its right-lateral slip rate being 5.1±1.2 mm/a. At the same time, SE of the Longmenshan fault, and the Deyucuo-Yinmahu fault shows some thrust motions. Based on previous studies, thick crust in the Longmen Mountains region makes the lower crust weaker than the surrounding areas. The southeastward flow of the weak lower crust, driven by the gravitational potential, is resisted by the strong crust of the Sichuan Basin, resulting in the uplifting of the Longmen Mountains and their sharp topographic contrast with the Sichuan Basin.

A few faults within the Sichuan-Yunnan block show strong tectonic deformation, such as the Litang fault slipping left-laterally at a rate of 4.4±1.3 mm/a and extending at a rate of 2.7±1.1 mm/a, and the Yunongxi fault zone shearing right-laterally at a rate of 2.7±2.3 mm/a and shortening at a rate of 6.7±2.3 mm/a.

We also notice three regions, Mabian-Yanjin, Simao-Pu'er, and Dayingjiang-Nantinghe, which are crosscut by conjugate faults. Our results reveal active deformation in these areas, but detailed strain distributions within the fault zones cannot be measured yet due to the spatial limitation of the current GPS station network in the regions.

In conclusion, driven by the north-northeastward indentation of the Indian plate into the Tibetan Plateau and the eastward gravitational push of the plateau, the southeast part of the plateau is extruded eastward. The motion is resisted by the stable South China block and turns to southeastward and then southward motions, resulting in the clockwise rotation of the Sichuan-Yunnan region around the eastern Himalayan syntaxis. A series of active faults have been developed along with the "crustal flow" process, such as the Xianshuihe-Xiaojiang fault zone delineating its eastern boundary and a broad right-lateral deformation zone behaving as the western boundary. Because of a mechanically weak crust, especially the lower crust, crustal deformation within the Sichuan-Yunnan block is characterized by relative motions between multiple micro-blocks, resulting in distributed deformation within the block, particularly along active faults forming the micro-block boundaries.

The authors are grateful to Deng Qidong, Xu Xiwei, Zhang Peizhen, Wang Qingliang, Wen Xueze, Zhang Zusheng, Wan Yongge, Zeng Yuehua, Song Fangmin, and Han Zhujun for their helpful suggestions and discussion.

1 Zhang P Z, Deng Q D, Zhang G M, et al. Active tectonic blocks and strong earthquakes in the continent of China. Sci China Ser D-Earth Sci, 2003, 46(Suppl): 13—24

2 Allen C R, Luo Z L, Qian H, et al. Field study of a highly active fault zone: The Xianshuihe fault of southwestern China. Geol Soc of Am Bull, 1991, 103: 1178—1199

3 Zhao G G, Liu D Q, Wei W, et a1. The late Quaternary slip rate and segmentation of the Xianshuihe active fault zone. In: Proceedings of

the PRC-USA Bilateral Symposium on the Xianshuihe Fault Zone, October 1990, Chengdu. Beijing: Seismological Press, 1992. 41－57
4 Sun J Z, Shi S Y. Inversion of the present kinematic characteristics of Xianshuihe fault zone from seismic moment tensor. Crustal Deformation Earthq (in Chinese), 1994, 14(4): 9－15
5 King R W, Shen F, Burchfiel B C, et al. Geodetic measurement of crustal motion in southwest China. Geology, 1997, 25(2): 179－182
6 Song F M, Wang Y P, Yu W X , et al. Xiaojiang Active Fault Zone (in Chinese). Beijing: Seismological Press, 1998. 237
7 Xiang H F, Guo S M, Xu X W, et al. Active block division and present-day motion features of the south region of Sichuan-Yunnan province. Seismol Geol (in Chinese), 2000, 22(3): 253－264
8 Shen C Y, Wang Q. GPS inversion of kinematic model of the main boundaries of the rhombus block in Sichuan and Yunnan. Chin J Geophys (in Chinese), 2002, 45(3): 352－361
9 Zhou R J, He Y L, Huang Z Z, et al. The slip rate and strong earthquake recurrence interval on the Qianning-Kangding segment of the Xianshuihe fault zone. Acta Seismol Sin (in Chinese), 2001, 23(3): 250－261
10 Zhou R J, He Y L, Yang T, et al. Slip rate and strong earthquake rupture on the Moxi-Mianning segment along the Xianshuihe-Anninghe fault zone. Earthq Res Chin (in Chinese), 2001, 17(3): 253－262
11 Shen J, Wang Y P, Ren J W. Quaternary right-lateral slip along the Dêqên-Zhongdian-Daju fault zone in Yunnan, China. In: Ma Z J, et al., eds. Contemporary Lithospherical Variation and Dynamic of Tibetan Plateau (3) (in Chinese). Beijing: Seismological Press, 2001. 123－135
12 He H L, Yasutaka I, Song F M, et al. Late quaternary slip rate of the Xiaojiang fault and its implication. Seismol Geol, 2002, 24(1): 14－26
13 Wen X Z, Xu X W, Zheng R Z, et al. Average slip-rate and recent large earthquake ruptures along the Garzê-Yushu fault. Sci China Ser D-Earth Sci, 2003, 46(Suppl): 276－288
14 Xu X W, Wen X Z, Zheng R Z, et al. Pattern of latest tectonic motion and its dynamics for active blocks in Sichuan-Yunnan region in China . Sci China Ser D-Earth Sci, 2003, 46(Suppl): 210－226
15 Wang Y P, Shen J, Wang Q, et al. On the lateral extrusion of Sichuan-Yunnan block. Earth Sci Front (in Chinese), 2003, 10(Suppl): 188－192
16 Qiao X J, Wang Q, Du R L. Characteristics of current crustal deformation of active blocks in the Sichuan-Yunnan region. Chin J Geophys (in Chinese), 2004, 47(5): 805－811
17 Tang W Q, Chen Z L. Present-day tectonics activity in the intersection area of the Xianshuihe fault and Longmenshan fault on the eastern margin of the Qinghai-Tibet Plateau. Geol Bull Chin (in Chinese), 2005, 24(12): 1169－1172
18 Xu X W, Zhang P Z, Wen X Z, et al. Features of active tectonics and recurrence behaviors of strong earthquakes in the western Sichuan province and its adjacent regions. Seismol Geol (in Chinese), 2005, 27(3): 446－461
19 Tapponnier P, Molnar P. Slip-line field theory and large-scale continental tectonics. Nature, 1976, 264: 319－324
20 Tapponnier P, Peltzer G, Le Dain A Y, et al. Propagating extrusion tectonics in Asia: New insights from simple experiments with plasticine. Geology, 1982, 10: 611－616
21 Peltzer G, Tapponnier P. Formation and evolution of strike-slip faults, rifts and basins during the India-Asia collision: An experimental approach. J Geophys Res, 1988, 93: 15085－15117
22 Avouac J P, Tapponnier P. Kinematic model of active deformation in central Asia. Geophys Res Lett, 1993, 20(10): 895－898
23 Peltzer G, Saucier F. Present day kinematics of Asia derived from geologic fault rates. J Geophys Res, 1996, 101: 27943－27956
24 Tapponnier P, Xu Z Q, Roger F, et al. Oblique stepwise rise and growth of the Tibet Plateau. Science, 2001, 294: 1671－1677
25 Replumaz A, Tapponnier P. Reconstruction of the deformed collision zone between India and Asia by backward motion of lithospheric blocks. J Geophys Res, 2003, 108(B6): 2285
26 England P, McKenzie D. A thin viscous sheet model for continental deformation. Geophys J R Astron Soc, 1983, 70: 295－321
27 Vilotte J P, Madariaga R, Daignières M, et al. Numerical study of continental collision: Influence of buoyancy forces and initial stiff inclusion. Geophys J R Astron Soc, 1986, 84: 279－310
28 Houseman G, England P. Crustal thickening versus lateral explosion in the Indian-Asian continental collision. J Geophys Res, 1993, 98: 12233－12249
29 England P, Molnar P. The field of crustal velocity in Asia calculated from Quaternary rates of slip on faults. Geophys J Int, 1997, 130: 551－582
30 Flesch L M, Haines A J, Holt W E. Dynamics of the India-Eurasia collision zone. J Geophys Res, 2001, 106: 16435－16460
31 Thatcher W. Microplate model for the present-day deformation of Tibet. J Geophys Res, 2007, 112, B01401, doi: 10.1029/2005JB004244
32 Chen Z, Burchfiel B C, Liu Y, et al. Global Positioning System measurements from eastern Tibet and their implications for India/Eurasia intercontinental deformation. J Geophys Res, 2000, 105: 16215－16227
33 Chen Z L, Shen F, Liu Y P, et al. The survey of GPS of crustal movement in the eastern Tibet Plateau regions. Chin Geol (in Chinese), 1998, 5: 32－35
34 Chen Z L, Zhang X Y, Shen F, et al. The monitoring of crustal movement in the southwest of China by GPS. Chin Sci Bull, 1999, 44(8): 851－854
35 Lu J N, Shen Z K, Wang M. Contemporary crustal deformation and active tectonic block model of the Sichuan-Yunnan region, China. Seismol Geol (in Chinese), 2003, 25(4): 543－554
36 Shen Z K, Lü J N, Wang M, et al. Contemporary crustal deformation around the southeast borderland of the Tibetan Plateau. J Geophys Res, 2005, 110, B11409, doi:10.1029/2004JB003421
37 Gan W J, Zhang P Z, Shen Z K, et al. Present-day crustal motion within the Tibetan Plateau inferred from GPS measurements. J Geophys Res, 2007, 112, B08416, doi:10.1029/2005JB004120
38 Wang M, Zhang Z S, Xu M Y, et al. Data processing and accuracy analysis of national 2000' GPS geodetic control network. Chin J Geophys (in Chinese), 2005, 48(4): 817－823
39 Wan Y G, Wang M, Shen Z K, et al. Co-seismic slip distribution of the 2001 west of Kunlun Mountain pass earthquake inverted by GPS and leveling data. Seismol Geol (in Chinese), 2004, 26(3): 393－404
40 Shen Z K, Zhao C, Yin A, et al. Contemporary crustal deformation in east Asia constrained by Global Positioning System measurements. J

Geophys Res, 2000, 105: 5721－5734
41 Niu Z J, Wang M, Sun H R, et al. The latest resutls of GPS velocity field in China. Chin Sci Bull, 2005, 50(9): 934－941
42 Okada Y. Surface deformation due to shear and tensile faults in a half-space. Bull Seismol Soc Am, 1985, 75: 1135－1154
43 Okada Y. Internal deformation due to shear and tensile faults in a half-space. Bull Seismol Soc Am, 1992, 82: 1018－1040
44 Zeng Y H, Shen Z K. Kinematic fault model of crustal deformation in California constrained by GPS observations. AGU Fall Meeting abstract, 2006
45 Jackson D D, Matsu'ura M. A bayesian approach to nonlinear inversion. J Geophys Res, 1985, 90: 581－591
46 Shen Z K, Ge B X, Jackson D D, et al. Northridge earthquake rupture models based on the global positioning system measurements. Bull Seismol Soc Am, 1996, 86: 37－48
47 Deng Q D, Zhang P Z, Ran Y K, et al. Basic characteristics of active tectonics of China. Sci China Ser D-Earth Sci, 2003, 46(4): 356－372
48 Wang E, Burchfiel B C. Late Cenozoic to Holocene deformation in southwestern Sichuan and adjacent Yunnan, China, and its role in formation of the southeastern part of the Tibetan Plateau. Geol Soc Am Bull, 2000, 112: 413－423
49 Meade B J, Hager B H. Block models of crustal motion in southern California constrained by GPS measurements. J Geophys Res, 2005, 110, B03403, doi:10.1029/2004JB003209
50 McCaffrey R. Block kinematics of the Pacific–North America plate boundary in the southwestern United States from inversion of GPS, seismological, and geologic data. J Geophys Res, 2005, 110, B07401, doi:10.1029/2004JB003307
51 Zhu A L, Xu X W, Zhou Y S, et al. Relocation of small earthquakes in western Sichuan, China and its implications for active tectonics. Chin J Geophys (in Chinese), 2005, 48(3): 629－636
52 Shen Z K, Wang M, Gan W J, et al. Contemporary tectonic strain rate field of Chinese continent and its geodynamic implications. Earth Sci Front (in Chinese), 2003, 10(Suppl): 93－100
53 Han W B, Jiang G F. Study on seismicity of daliangshan and Anninghe-Zemuhe fault zones. J Seismol Res (in Chinese), 2005, 28(3): 207－212
54 Western Yunnan Earthquake Prediction Test Site, Yunnan Seismological Bureau. The 1996 Lijiang Earthquake (in Chinese). Beijing: Seismological Press, 1998. 188
55 Institute of Geology State Seismological Bureau, Yunnan Seismological Bureau. Active Faults in Northwestern Yunnan Region (in Chinese). Beijing: Seismological Press, 1990
56 Sun J, Xu C F, Jiang Z, et al. Relationship between the electrical structure of crust and lower lithosphere and crustal tectonics in west Yunnan region. Seismol Geol (in Chinese), 1989, 11(1): 35－45
57 Zhou R J, Chen G X, Li Y, et al. Research on active faults in Litang-Batang region, western Sichuan province, and the seismogenic structures of the 1989 Batang *M*6.7 earthquake swarm. Seismol Geol (in Chinese), 2005, 27(1): 31－43
58 Burchfiel B C. New technology: New geological challenges. GSA Today, 2004, 14(2): 4－10
59 Xiang H F, Xu X W, Guo S M, et al. Sinistral thrusting along the Lijiang-Xiaojinhe fault since Quaternary and its geologic-tectonic significance —— Shielding effect of transverse structure of intracontinental active block. Seismol Geol (in Chinese), 2002, 22(2): 188－198
60 Huang W, Zhou R J, He Y L, et al. Holocene activity on Yunongxi fault and Liuba M6.2 earthquake in Kangding, Sichuan. Earthquake Res Chin (in Chinese), 2000, 16(1): 53－59
61 Chen G H. Structural transformation and strain partitioning along the northeast boundary belt of the Sichuan-Yunnan block. Dissertation for Doctoral Degree (in Chinese). Beijing: Institute of Geology, China Earthquake Administration, 2006
62 Zhang S M, Nie G Z, Liu X D, et al. Kinematical and structural patterns of Yingjing-Mabian-Yanjin thrust fault zone, southeast of Tibetan Plateau, and its segmentation from earthquakes. Seismol Geol (in Chinese), 2005, 27(2): 221－233